

Microhollow Cathode Discharge Reactor Chemistry

David D. Hsu¹ and David B. Graves^{1,2}

Received August 8, 2003; revised May 3, 2004

We discuss the microhollow cathode discharge (MHCD) as a microreactor for endothermic reactions. The high-peak neutral temperature, power density, and ion density of MHCDs may provide a highly reactive environment for these chemistries. Decomposition of ammonia and carbon dioxide are examined. Conversion is found to vary strongly based mainly on residence time. The results are fit to a plug-flow reactor model, and an effective reaction temperature is calculated. The effective reaction temperature in both cases exceeds 2000 K and suggests that thermal processes play an important role in decomposition.

KEY WORDS: Microhollow cathode; microplasma; microreactor; decomposition.

1. INTRODUCTION

Microhollow cathode discharges (MHCDs), because of their small size and high-pressure stability, could be used as a microreactor to process gases. Such microreactors have appeared on so-called 'lab-on-a-chip' configurations, where entire analytical chemical processes, such as DNA PCR, can be miniaturized onto devices smaller than the size of a human hand.⁽¹⁾ This line of thought can be extended to entire chemical processes where a 'system-on-a-chip' could produce small amounts of a chemical point-of-use and on-demand.⁽²⁾ As the '-on-a-chip' and other microelectromechanical systems (MEMS) technologies mature, microreactors will become more prominent.

The MHCD properties imply that the discharge could be well-suited as a microreactor, particularly for certain classes of reactions. The discharge has a high-power density. These plasmas typically operate at 1–5 W per hole. Simply dividing the power deposited by the hole volume yields a high-power density on the order of several kw/cm³. By comparison, the analogous calculation on an inductively coupled plasma (ICP) yields a

¹Department of Chemical Engineering, University of California at Berkeley, Berkeley, CA 94720.

²To whom correspondence should be addressed. E-mail: graves@uclink4.berkeley.edu



31 power density on the order of 0.1 W/cm^3 . One would expect that high-
 32 power densities would result in high-peak neutral temperatures in the
 33 MHCD. As shown by optical emission thermometry measurements of the
 34 plasma, the peak neutral temperature is of the order of $1000\text{--}2000 \text{ K}$.^(3,4)
 35 The high-power density and peak neutral temperature would be ideal for
 36 endothermic ($\Delta H_{rxn} > 0$) reactions. High temperatures also would pro-
 37 mote the kinetics of a reaction by increasing the Arrhenius rate coeffi-
 38 cients. The high gas temperatures are likely the result of the direct current
 39 (DC) nature of the discharge in which ion and electron current through
 40 the gas (especially in the cathode fall) efficiently transfers energy to the
 41 neutral gas. Higher gas pressures available to MHC operation increase
 42 equilibrium conversion for mole-decreasing reactions. In addition, reac-
 43 tions could be enhanced by reactive plasma species. Plasma densities have
 44 been measured as high as 10^{15} cm^{-3} .⁽⁴⁾

45 Few other, if any, high-pressure plasmas can achieve such high
 46 temperatures on such a small scale. In dielectric barrier discharge and
 47 coronas, neutral gas temperatures are relatively low, thus chemistry is gen-
 48 erally thought to be a result of electron-impact processes. As the charac-
 49 teristic dimension of the plasma is on the order of 10^{-4} m , temperature
 50 gradients are likely to be on the order of 10^7 K/m . In a typical ICP, char-
 51 acteristic dimensions are usually at least two orders of magnitude higher,
 52 resulting in smaller peak gradients of 10^5 K/m . Gradients in other plasma
 53 quantities are also likely to be large in MHC's, suggesting that relatively
 54 small changes in device design could have significant effects on plasma
 55 performance. The key characteristics of the MHC plasma from the point
 56 of view of chemical reactions are their very compact size coupled with
 57 their extraordinarily high intensity. There are few alternative configura-
 58 tions that couple the size and intensity of the MHC. Thin-film resistive
 59 heaters used in MEMS achieve temperatures greater than 1000 K , but suffer
 60 from material degradation.⁽⁵⁾

61 Endothermic reactions were chosen to study the effectiveness of the
 62 MHCD as a microreactor. The chemistries and enthalpies are listed in
 63 Table 1. The destruction of ammonia into nitrogen and hydrogen (the
 64 reverse of the well-known Haber process) could be used as a source of a
 65 hydrogen. The cracking of carbon dioxide could be used as part of a

Table I. Chemistries Studied and Relevant Thermodynamic Data

Chemistry	Enthalpy (KJ/mol)
$\text{NH}_3 \rightarrow \frac{1}{2}\text{N}_2 + \frac{3}{2}\text{H}_2$	$\Delta H^0 = 46$
$\text{CO}_2 \rightarrow \text{CO} + \frac{1}{2}\text{O}_2$	$\Delta H^0 = 283$

66 method to dispose of radioactive carbon dioxide resulting from nuclear
67 fuel production⁽⁶⁾ or for the production of oxygen.

68 2. EXPERIMENTAL

69 The MHC used in this work is based on the early studies of Schoen-
70 bach *et al.*^(7,8) The MHC is constructed from two molybdenum electrodes
71 sandwiching a mica dielectric (Fig. 1). Molybdenum is used as an elec-
72 trode because of its low work function and high sputtering threshold.⁽⁹⁾
73 The molybdenum electrodes are $100\ \mu\text{m}$ thick. The dielectric is $260\ \mu\text{m}$
74 thick. The three layers are epoxied together, and a hole $200\ \mu\text{m}$ in diame-
75 ter is mechanically drilled through all three layers.

76 The cathode is supplied with a negative DC voltage through a $100\ \text{k}\Omega$
77 ballast resistor. The anode is grounded through a $100\ \Omega$ resistor. The
78 plasma current is determined by measuring the voltage drop across the
79 $100\ \Omega$ resistor. The plasma voltage is found by measuring the voltage at
80 the MHC with respect to ground.

81 The apparatus used for microreactor studies is shown in Fig. 2. The
82 gas flow is controlled by a mass flow controller. The gas flows through
83 the microhollow cathode discharge. The bulk of the gas flow exits to
84 a mechanical pump, bypassing any analytical tools. A metering valve
85 upstream of the mechanical pump is adjusted to control the pressure for
86 a given flowrate. Most of the tubing used is $6.4\ \text{mm}$ diameter stainless
87 steel tubing so as to minimize the volume of the system. Two capaci-
88 tance manometer pressure gauges monitor pressure upstream and down-
89 stream of the MHC. The MHC is clamped in place by a fiberglass holder.
90 Two concentric o-rings on each side of the MHC minimize leakage. The
91 cathode is oriented downstream of the anode. Some of the gas bleeds
92 through leak valves to an Inficon Transceptor 2 mass spectrometer or a

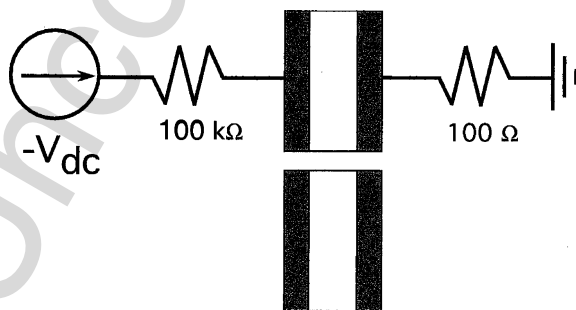


Fig. 1. Microhollow cathode and electrical circuit.

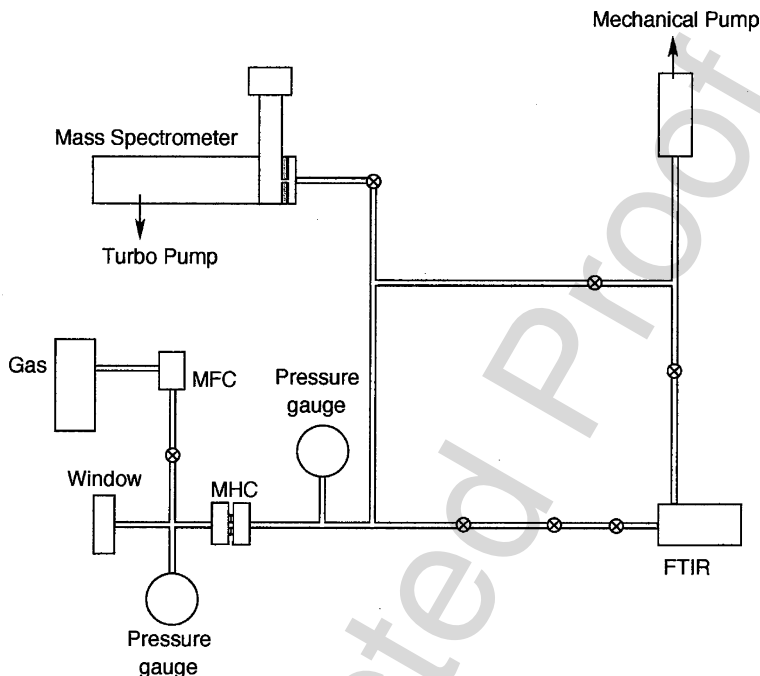


Fig. 2. Apparatus for microreactor studies allowing for simultaneous mass spectrometer and Fourier transform infrared (FTIR) measurements.

93 MKS On-Line 2010 Fourier transform infrared (FTIR) spectrometer. The
 94 mass spectrometer, pumped by a turbo pump, operates at pressures of
 95 1×10^{-6} – 1×10^{-5} Torr. The FTIR, with a sampling volume of 1600 cm^3
 96 operates at a few Torr. Operating the FTIR at low pressure allows for
 97 concentrations in the sampling volume to reach steady state more quickly
 98 than if it were operating at high pressures of the MHC. IR is absorbed
 99 by some absolute number of molecules in the gas cell. The MKS software
 100 calculates the density based on the spectra. The pressure in the FTIR gas
 101 cell is a few Torr, lower than the hundreds of Torr near the MHC. The
 102 measured density will be based then only on a representative fraction of
 103 the molecules exiting the MHC, and it is assumed that the flow never is
 104 molecular flow as the mean free path is much smaller than tube and valve
 105 dimensions. A lumped conductance model, described in Section 4, of the
 106 experimental system is developed to verify that the FTIR readings reflect
 107 the concentrations in the system and that the resulting percent conversions
 108 are accurate. The model is also used to explain surges and dips in the mass
 109 spectrometer and FTIR readings.

110 Two MHCs are also used to test conversion in a series of reactors
111 (Fig. 3). The second plasma may increase the conversion as reactive spe-
112 cies may be carried over to the second plasma. The second plasma would
113 also operate at a lower pressure, and thus operate more stably at a given
114 power. Both MHC's are put in the holder shown in Fig. 2. An o-ring
115 2.5 mm in thickness is placed between the two MHC's. Each MHC has an
116 electrical circuit independent of the other one, but both have power sup-
117 plies delivering negative voltage through a 100 k Ω ballast resistor. The two
118 grounded anodes face each other in the center of the series system in order
119 to avoid plasma formation between the two MHC's.

120 3. RESULTS

121 3.1. Ammonia

122 The results of cracking ammonia are charted in both the mass spec-
123 trometer and the FTIR. Figure 4 shows the mass spectrometer results of
124 one run. The plasma is turned on and off repeatedly to demonstrate the
125 conversion of ammonia. The hydrogen and nitrogen signals in the mass
126 spectrometer increase when the plasma is on. The ammonia signals in the
127 FTIR show a similar response, but hydrogen and nitrogen are not seen
128 in the FTIR because the FTIR cannot detect homonuclear diatomic mole-
129 cules. By taking the steady-state levels of ammonia when the plasma is
130 on and when the plasma is off, a percent conversion can be calculated.
131 The percent conversion calculated for the FTIR signal is consistent with
132 the value calculated for the mass spectrometer signal. The nitrogen, hydro-
133 gen and ammonia signals in the mass spectrometer cannot be compared
134 quantitatively to each other because of different mass spectrometer sensi-
135 tivities to different molecules. Thus, one cannot assume from Fig. 4 that
136 10 times more hydrogen is produced compared with nitrogen. The ratios
137 of the different gases in the mass spectrometer also vary from run to run

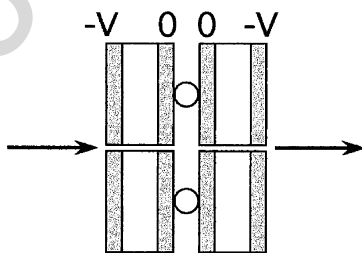


Fig. 3. Microhollow cathode's in series.

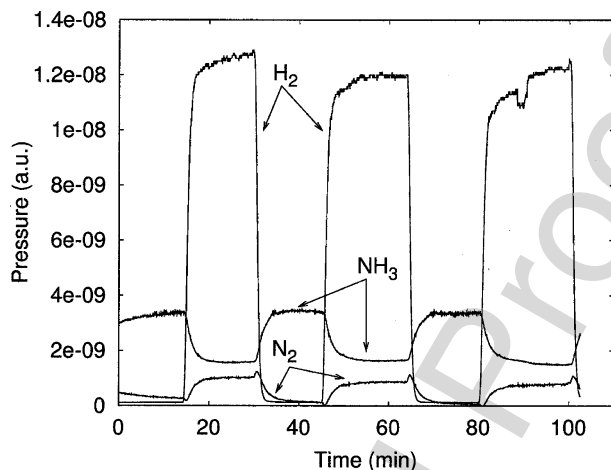


Fig. 4. Mass spectrometer results of ammonia decomposition in a microhollow cathode. Ammonia flow is at 1.5 sccm, with an upstream pressure of 100 Torr. The voltage of the plasma is 480 V and the current is 9 mA.

138 so a quantitative analysis of the amount of hydrogen and nitrogen
139 produced was not possible.

Conversions for ammonia for different flowrates are shown in Fig. 5. As the flowrate increases, the conversion drops. The conversion data can

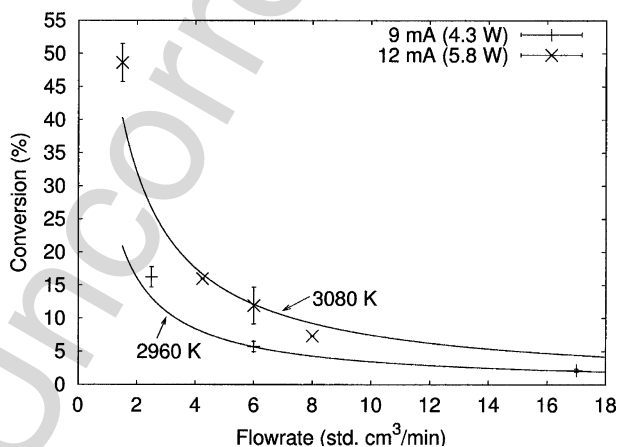


Fig. 5. NH_3 conversion as a function of flowrate for two microhollow cathode powers. Upstream pressure is 100 Torr.

be fit to a plug flow reactor model and kinetic data from the literature.^(10,11) Davidson *et al.*⁽¹⁰⁾ provide a pyrolysis mechanism with 21 elementary steps. Konnov and DeRuyck⁽¹¹⁾ list 50 elementary steps. In order to obtain a first-order rate equation of the Arrhenius form

$$-\frac{d[\text{NH}_3]}{dt} = k_0 \exp\left(-\frac{E}{RT}\right) [\text{NH}_3], \quad (1)$$

ammonia conversions are calculated for both models for temperatures from 2000 to 3000 K and for reaction times of 10^{-4} and 10^{-5} s using Kineticus reaction simulation software. The temperature range is chosen to be near the temperature range tested experimentally in the Davidson paper. Although for an ordinary first-order equation, the rate expression should not change with different residence times, the expressions for both literature mechanisms change slightly. The resulting activation energies, E , and pre-exponential factors, k_0 , from the two different rate mechanisms and two different residence times are averaged to obtain the following rate expression:

$$-\frac{d[\text{NH}_3]}{dt} = 4.23 \times 10^{13} \text{s}^{-1} \exp\left(\frac{-5.19 \times 10^5 \text{J mol}^{-1}}{RT}\right) [\text{NH}_3] \quad (2)$$

140 where R is the universal gas constant [$8.314 \text{J (mol}\cdot\text{K)}^{-1}$] and T is the tem-
141 perature in Kelvin.

A plug-flow reactor assumes gas goes through the reactor as a ‘plug’ and there is no axial diffusion. The plug-flow reactor design equation,

$$V = v[\text{NH}_3] \int_0^X \frac{dX}{-d[\text{NH}_3]/dt}, \quad (3)$$

can be solved for conversion, X :

$$X = 1 - \exp\left[k_0 \exp\left(-\frac{E}{RT}\right) \tau\right] \quad (4)$$

142 where V is the volume of the reactor, v is the volumetric flowrate, and τ
143 is the residence time. As the residence time for the reaction is small, the
144 reaction conversion does not change much if the reactor were modeled as
145 a continuously stirred tank reactor.

146 The model assumes that the reaction occurs only in the MHC cylin-
147 drical hole and decomposition results from solely thermal processes. The
148 residence time is calculated for the gas velocity going through a reactor
149 $500 \mu\text{m}$ long. In addition to affecting the rate constant of the reaction,
150 the temperature also affects the density of the gas. To conserve mass flow,

151 the velocity of the gas in the reactor will change. With a change in gas
152 velocity, the residence time of the reaction changes. The reaction temper-
153 ature then must be calculated to satisfy both the reaction kinetics and the
154 residence times used to calculate the reaction kinetics. The calculations are
155 iterated until a self-consistent reaction temperature is obtained. The model
156 does not take into account the change in moles of gas with reaction.

157 For the data at an upstream pressure of 100 Torr and power of 4.3 W
158 in Fig. 5, the calculated reaction temperature is 2960 K. For the same
159 pressure but a power of 5.8 W, the calculated temperature is 3080 K. The
160 33% increase in power increased the reaction temperature by only 4%.

161 These calculated temperatures are higher than the reported temper-
162 atures of 1000–2000 K. For purely thermal ammonia decomposition
163 occurring at 2000 K and the residence times tested, less than 0.01% of
164 the ammonia would be converted. There are a few possible reasons for
165 this discrepancy. Reactive plasma species, such as ions and radicals, may
166 enhance the reaction to boost the effective reaction temperature. In addi-
167 tion, the reaction is not limited to the MHC hole. OES temperature mea-
168 surements were conducted in nitrogen, not ammonia.

169 An increase in the pressure from 100 to 700 Torr increases conversion
170 (Fig. 6). This is expected because at a higher pressure, a lower gas velocity
171 is needed to deliver the same standard flowrate. With a lower gas velocity,
172 the residence time is higher. Even though the conversion increased for a
173 higher pressure, the data are close to the same temperature as the lower

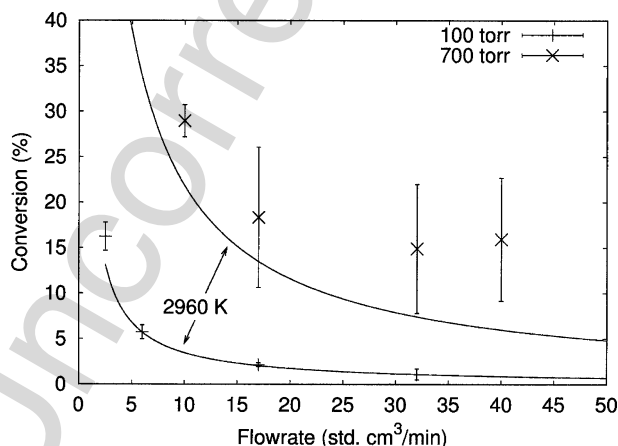


Fig. 6. NH_3 conversion as a function of flowrate and pressure. An increase in pressure increases the conversion by increasing the residence time for the same standard flowrate. The 100 Torr data points are the same as 4.3 W points in Fig. 5.

174 pressure data, as the residence time for the 700 Torr case is seven times
175 longer than the 100 Torr case. If the data are plotted against residence
176 time instead of flowrate as in Fig. 7, the data are near the conversion
177 predicted by the thermal decomposition model. Larger error was present
178 with 700 Torr runs at higher flowrates. This may have been a result of
179 larger pressure increases in the system with the plasma on. While part of
180 the increased conversion may be a result of increased current densities at
181 higher pressures,⁽¹²⁾ the ammonia conversion did not increase proportion-
182 ally to the square of the pressure. Thus, the effect of residence time is
183 likely the most significant factor.

184 3.2. Carbon dioxide

185 The cracking of carbon dioxide by MHC is measured by both mass
186 spectrometer and FTIR. Figure. 8 shows the results of one run in the
187 mass spectrometer. Similar results were seen in the FTIR. Although car-
188 bon monoxide could decompose to form carbon and oxygen, the further
189 decomposition of carbon monoxide does not exceed 35% even under reac-
190 tion temperatures as high as 7500 K.⁽¹³⁾ In our analysis, decomposition
191 of carbon monoxide is neglected. The steady state levels of carbon diox-
192 ide while the plasma was on and off are used to calculate conversion.

As in the ammonia experiments, the effect of flowrate on conver-
sion is studied. As the flowrate increases, the conversion of carbon dioxide
decreases (Fig. 9). An increase in up-stream pressure from 150 to 250 Torr
increases conversion. The upstream pressure of 250 Torr is the maximum

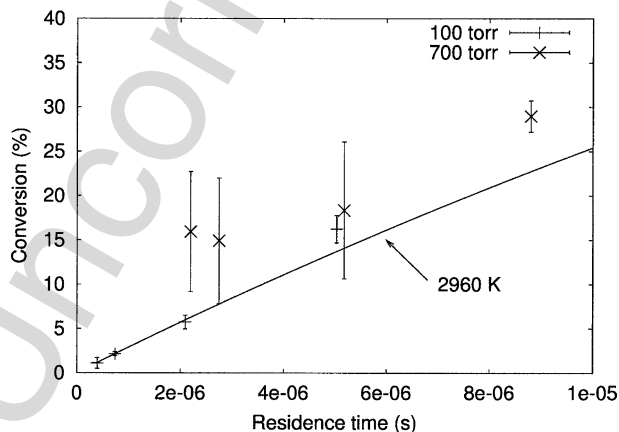


Fig. 7. NH_3 conversion as a function of residence time for the same data shown in Fig. 6.

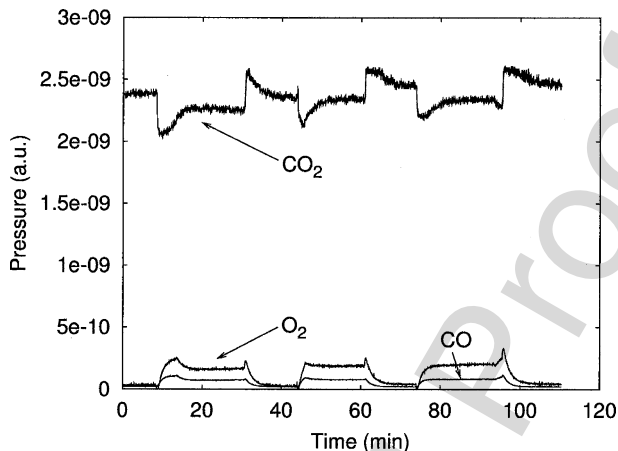


Fig. 8. Mass spectrometer signals of carbon dioxide decomposition for 19 sccm, 150 Torr upstream pressure and 5.2 W. When the plasma is on, carbon dioxide decreases, while carbon monoxide and oxygen increase.

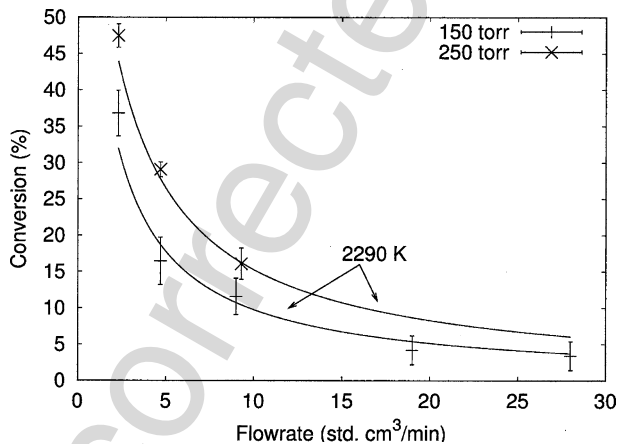


Fig. 9. CO₂ conversion as a function of flowrate for two operating pressures. Both sets of data are fit to the same effective reaction temperature.

pressure which would allow steady-state operation. The data are fit to a plug-flow reactor model and the kinetic data.⁽¹⁴⁾ The kinetic dissociation rate, k_d , for the reaction is

$$k_d = 7.5 \times 10^{12} T^{\frac{1}{2}} \exp\left(-\frac{1.04 \times 10^5}{RT}\right) \frac{\text{cm}^3}{\text{mol} \cdot \text{s}}. \quad (5)$$

193 The reaction temperature is calculated for carbon dioxide decomposi-
 194 tion in the same manner that the temperature is calculated for ammonia
 195 decomposition. Both the data from the 150 and 250 Torr experiments cor-
 196 respond to a reaction temperature of 2290 K. As in the ammonia experi-
 197 ments, we see a high reaction temperature.

198 3.3. MHCD's in Series

199 The results of runs when operating two plasmas in series are shown in
 200 Fig. 10 and Table II. The conversion with both plasmas on is the summa-
 201 tion of the individual conversions of each plasma. Although no enhance-
 202 ment of the reaction occurs, the results suggest that when several of these
 203 plasmas are put in series, the conversion would be equivalent to a reactor
 204 volume equal to the summation of the individual plasma volumes. Sub-
 205 sequent plasmas also operate at lower pressure and could thus operate at
 206 lower powers. This is consistent with a plug-flow reactor model.

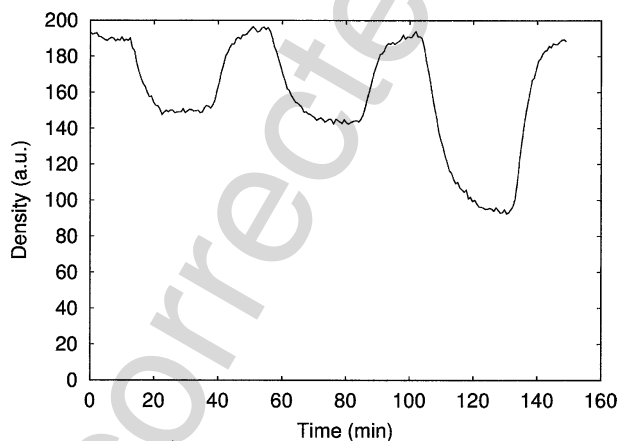


Fig. 10. Fourier transform infrared (FTIR) results of NH_3 decomposition with plasmas in series at 4.7 W, 110 Torr upstream pressure. The first decrease in signal is a result of only the upstream plasma. The second decrease is a result of only the downstream plasma. The third decrease is a result of both plasmas on.

Table II. Conversion of Ammonia in Microhollow Cathode's Discharges in Series

	Upstream	Downstream	Both
Conversion (%)	6.8 ± 2.2	8.9 ± 1.0	16.3 ± 3.0

207 3.4. Pressure and MHC-Lumped Conductance Model

208 In order to confirm the interpretation of the FTIR and mass spec-
 209 trometer data, a model of the flows and conductances of the apparatus is
 210 used. The model could be used to determine whether the surges and dips
 211 in mass spectrometer data in Fig. 8 are a result of the temperature changes
 212 in the MHC or actual changes in gas density. Most importantly, the model
 213 would confirm that the difference in the reading with the plasma off and
 214 the reading with the plasma on is indeed the percent conversion, rather
 215 than an artifact of changes in pressure or factors not related to gas den-
 216 sity.

217 Additionally, the plasma affects the pressure in the system and such
 218 effects would have process design implications. When the plasma is on,
 219 the pressure upstream of the plasma rises to a new steady state, and
 220 the pressure downstream of the plasma will decrease initially. When the
 221 plasma is turned on, the temperature in the region rises. An increase in
 222 temperature decreases gas density. In order to maintain the same mass
 223 flowrate, the pressure drop must increase. Such phenomena have been
 224 explained and modeled using finite element analysis.⁽¹⁵⁾ The lumped con-
 225 ductance model would verify whether the pressure changes seen in the
 226 system are the result of a decrease in conductance after turning on the
 227 plasma.

The geometry used to model the experimental apparatus (Fig. 2) is shown in Fig. 11. This consists of two volumes, of sizes V_0 and V_1 and at pressures of P_0 and P_1 , respectively. These volumes are connected by the MHC orifice, modeled as a volumeless section with a conductance of C_1 . A flowrate of Q_0 is fed to V_0 . The system is pumped out by a pump at constant pressure, P_p , connected to V_1 , by a valve of conductance, C_v . The volumes are isothermal; a rise in the temperature of the MHC orifice is assumed not to have an effect on the temperatures of the surrounding volumes. This system can be described by the ordinary differential equations shown in Eqs. (6) and (7):

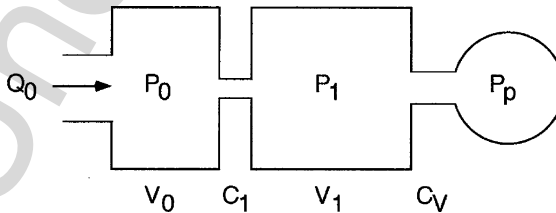


Fig. 11. Two-volume geometry used in lumped conductance model.

$$Q_0 - C_1(P_0 - P_1) = V_0 \frac{dP_0}{dt} \quad (6)$$

$$C_1(P_0 - P_1) - C_v(P_1 - P_p) = V_1 \frac{dP_1}{dt} \quad (7)$$

228 We can determine experimentally the conductances of the orifice and
 229 valve, given the flowrate and the pressure drops at steady state. Flowrates
 230 of 0.201 and 0.401 Torr-L/s (15.8 and 31.7 sccm, respectively) of nitrogen
 231 were used. The upstream pressure, P_0 , was measured by a convection gauge,
 232 and the downstream pressure, P_1 , was measured by a capacitance manom-
 233 gauge. The resulting pressures are shown in Fig. 12. The pressure changes
 234 for the convection gauge were not as smooth as for the capacitance manom-
 235 eter. The convection gauge, at pressures around 200 Torr, was only accurate
 236 to ± 5 Torr. The pump pressure, P_p , is 60 m Torr.

237 The volumes and conductances of each section are solved using
 238 Eqs. (6) and (7). The slopes of the pressure curves at various times are
 239 used for the derivative terms to calculate the volume. These volumes are
 240 averaged. The resulting conductances and volumes are listed in Table III.

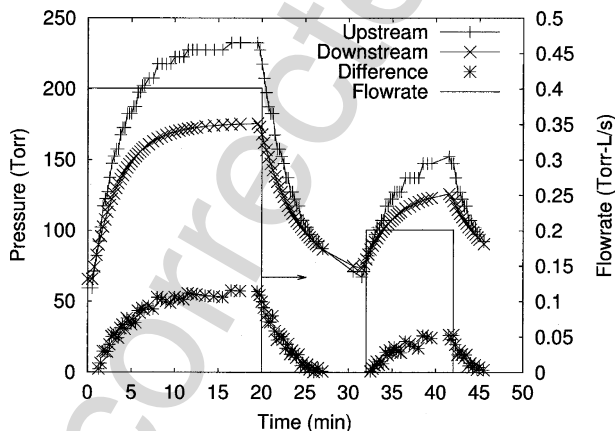


Fig. 12. Pressure changes with a flowrate of 0.401 Torr L/s from 0 to 20 min and a flowrate of 0.201 Torr L/s from 32 to 42 min.

Table III. Experimental Values of Conductance Model Parameters

Parameter (unit)	Average
C_1 (L/s)	0.00739
C_v (L/s)	0.00192
V_0 (L)	0.00789
V_1 (L)	0.014

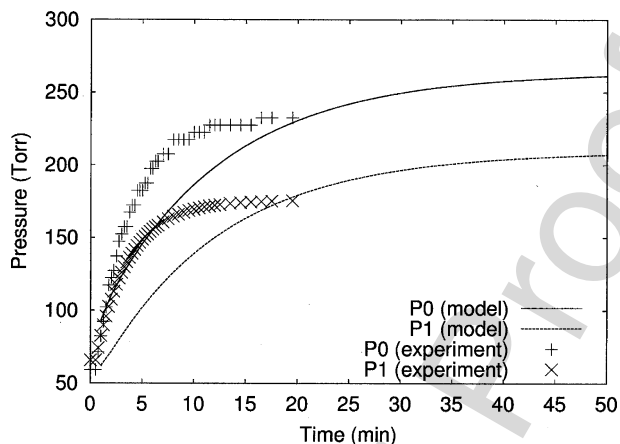


Fig. 13. Experimental and simulated pressure increases for both volumes with a flowrate of 0.401 Torr L/s.

241 The pressure increases are simulated by solving the system of two
 242 ordinary differential equations, Eqs. (6) and (7). The simulated pressure
 243 increases are shown in Figs. 13 and 14. For the lower flowrate, the simulation
 244 underestimates the steady-state pressures by approximately 30 Torr
 245 for both volumes. For the higher flowrate, the simulation overestimates
 246 the steady-state pressures by approximately 30 Torr for both volumes. The
 247 shapes of the pressure curve are similar as those found in experiment. The

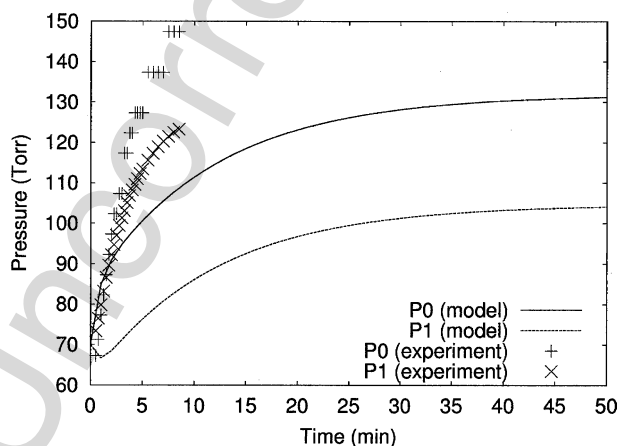


Fig. 14. Experimental and simulated pressure increases for both volumes with a flowrate of 0.201 Torr L/s.

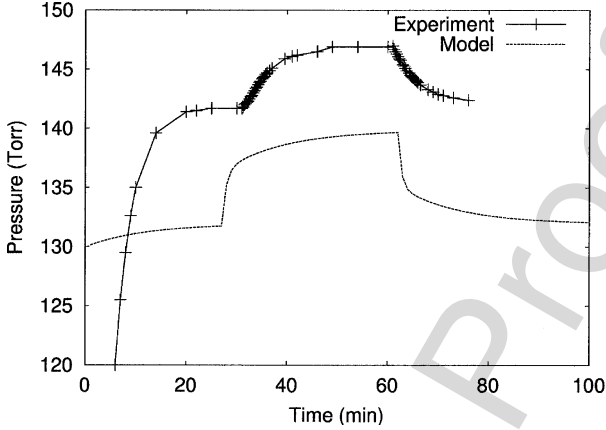


Fig. 15. Experiment and model comparison of P_0 , turning on a plasma at 31 min (model turns on at 27 min) and turning off the plasma at 62 min.

248 times to reach 95% of the steady-state pressures are approximately 21 min
 249 longer than those found in the experiment.

250 The change in the conductance of the orifice, C_1 , when a plasma
 251 is turned on is also tested. In an experiment, a plasma in a flow of
 252 0.201 Torr-L/s of nitrogen is turned on, and the pressures in both volumes
 253 is monitored. The pressures are measured with a capacitance manometer
 254 in two separate experiments. These results are represented as points in
 255 Figs. 15 and 16.

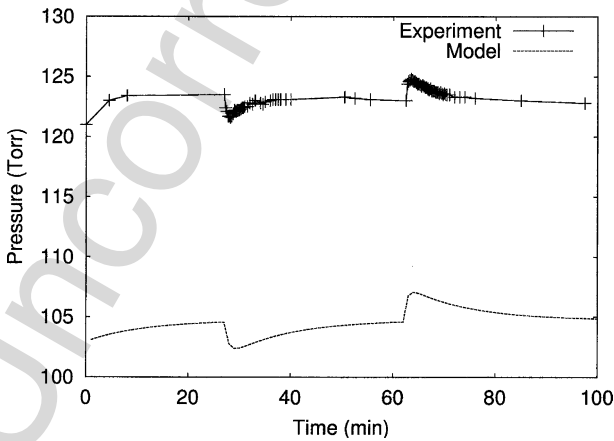


Fig. 16. Experimental and model comparison of P_1 , turning on the plasma at 27 min and off at 62 min.

256 When the plasma is turned on, the upstream pressure increases as
257 a result of the decreased conductance of the orifice. This can be seen
258 in Eq. (6). The system is initially at a steady-state pressure. When the
259 conductance, C_1 , decreases, dP_0/dt becomes positive. However, the down-
260 stream pressure, P_1 , drops initially when the plasma is turned on. As
261 shown in Eq. (7), when C_1 drops, dP_1/dt must be negative. As the
262 upstream pressure increases, the $C_1(P_0 - P_1)$ term eventually equals Q_0 .
263 With those terms equal, Eq. (7) will be the same as when the system was
264 at steady state and the plasma was off. P_1 must then return to the same
265 pressure as when the plasma was off.

266 In our model, the plasma is turned on at 27 min (to coincide with
267 the run measuring P_1) thereby decreasing the conductance of the orifice.
268 In this case, the conductance decreases by a factor of 1.29, from 0.00192
269 to 0.00149 L/s. This conductance is chosen to match the magnitudes of the
270 pressure changes found experimentally. The plasma is turned off at 62 min,
271 increasing the conductance back to the original value. The model results
272 are shown in Figs. 15 and 16. The simulated shapes of the pressure curves
273 are similar to those found in experiments. As noted earlier, the calculated
274 times to reach the initial steady state when flowing in the gas with no
275 plasma on is longer than in experiment. However, once this steady state
276 is reached, the response of the pressures in the model to a change in con-
277 ductance is similar to what is found in experiment. As both the mass spec-
278 trometer and FTIR sample from gas downstream of the plasma, Fig. 16
279 shows that any change in the steady-state readings of the FTIR and the
280 mass spectrometer are the result of concentration changes and not pres-
281 sure changes.

282 This simple lumped conductance model verifies that changes in pres-
283 sure seen experimentally are a result of a change in conductance of the
284 MHC orifice. The cause of the change in conductance is presumably the
285 result of temperature changes because of the plasma.

286 4. CONCLUSIONS

287 The experiments presented in this paper showed significant decom-
288 position of NH_3 and CO_2 , occurring with effective reaction tempera-
289 tures exceeding 2000 K. Based on these results, thermal processes play
290 an important role in the reaction chemistry in the MHCD. A simple
291 model based only on thermal decomposition can be used to effectively pre-
292 dict the conversion response as a result of the changes in flow rate and
293 pressure. However, because the effective reaction temperatures are higher
294 than the reported temperatures for MHCD's, it seems likely that part of
295 the decomposition kinetics are because of the reactive plasma ions and

296 electrons, in addition to purely thermal processes. Experiments with more
297 than one MHC in series increase conversion significantly. Pressure changes
298 are observed in the volumes upstream and downstream of the plasma
299 when the plasma was toggled on or off. Such behavior is modeled with
300 a lumped conductance model, which relates the pressure behavior to a
301 decrease in conductance with the plasma on, which would be consistent
302 with the MHCD increasing the temperature in the discharge hole. The
303 conversions seen in the MHCD in these experiments are lower than what
304 could be achieved in a lower temperature, but larger, microreactors. How-
305 ever, the MHCD has a high reaction temperature occurs in a naturally
306 small space, without the need to scale down, unlike with resistive heat-
307 ers. This key advantage could be exploited as ‘on-a-chip’ systems become
308 smaller and smaller.

309 ACKNOWLEDGMENTS

310 The authors thank Heywood Kan and Chad Su for experimental
311 assistance. This work is supported in part by Kodak and a National Sci-
312 ence Foundation fellowship.

313 REFERENCES

- 314 1. M. Freemantle, *Chem. Eng. News* **77**, 27 (1999).
- 315 2. R. Srinivasan et al., *Am. Inst. Chem. Eng. J.* **43**, 3059 (1997).
- 316 3. F. Leipold, R. H. Stark, A. El-Habachi, and K. H. Schoenbach, *J. Phys. D: Appl.*
317 *Phys.* **33**, 2268 (2000).
- 318 4. C. Penache et al., *Plasma Sources Sci. Technol.* **11**, 476 (2002).
- 319 5. S. L. Firebaugh and M. A. Schmidt, *J. Microelectromech. Syst.* **7**, 128 (1998).
- 320 6. T. Sakurai and A. Yokoyama, *J. Nucl. Sci. Tech.* **37**, 814 (2000).
- 321 7. K. H. Schoenbach, R. Verhappen, T. Tessnow, and F. E. Peterkin, *Appl. Phys. Lett.*
322 **68**, 13 (1996).
- 323 8. K. H. Schoenbach, A. El-Habachi, W. Shi, and M. Ciocca, *Plasma Sources Sci. Tech-*
324 *nol.* **6**, 468 (1997).
- 325 9. A. D. White, *J. Appl. Phys.* **30**, 711 (1959).
- 326 10. D. F. Davidson, K. Kohse-Höinghaus, A. Y. Chang, and R. K. Hanson, *Intl. J. Chem.*
327 *Kinet.* **22**, 513 (1990).
- 328 11. A. A. Konnov and J. DeRuyck, *Combust. Sci. Tech.* **152**, 23 (2000).
- 329 12. M. Moselhy, W. Shi, R. H. Stark, and K. H. Schoenbach, *IEEE Trans. Plasma Sci.*
330 **30**, 198 (2002).
- 331 13. Y. Nishimura, T. Takenouchi, and W. Sakai, *Bull. Chem. Soc. Jap.* **47**, 2331 (1974).
- 332 14. N. A. Ebrahim and R. J. Sandeman, *J. Chem. Phys.* **65**, 3446 (1976).
- 333 15. M. A. Nierode, Neutral Gas Pressure Profiles in Flowing, Non-equilibrium Plasmas,
334 Master's Thesis, University of California, Berkeley, CA, 2003.